IOPscience iopscience.iop.org

Home Search Collections Journals About Contact us My IOPscience

Dissociation dynamics of ethylene molecules on a Ni cluster using *ab initio* molecular dynamics simulations

This content has been downloaded from IOPscience. Please scroll down to see the full text.

2016 J. Phys.: Condens. Matter 28 145001

(http://iopscience.iop.org/0953-8984/28/14/145001)

View the table of contents for this issue, or go to the journal homepage for more

Download details:

IP Address: 133.30.125.154
This content was downloaded on 08/03/2016 at 13:27

Please note that terms and conditions apply.

IOP Publishing Journal of Physics: Condensed Matter
J. Phys.: Condens. Matter **28** (2016) 145001 (11pp) doi:10.1088/0953-8984/28/14/145001

Dissociation dynamics of ethylene molecules on a Ni cluster using *ab initio* molecular dynamics simulations

K Shimamura[1,2], Y Shibuta[3], S Ohmura[4], R Arifin[5] and F Shimojo[1]

[1] Department of Physics, Kumamoto University, 2-39-1 Kurokami, Chuo-ku, Kumamoto 860-8555, Japan
[2] Graduate School of System Informatics, Kobe University, 1-1 Rokkodai, Nada-ku, 657-8501, Japan
[3] Department of Materials Engineering, The University of Tokyo, 7-3-1 Hongo, Bunkyo-ku, Tokyo 113-8656, Japan
[4] Research Center for Condensed Matter Physics, Hiroshima Institute of Technology, 2-1-1, Miyake, Saeki-ku, Hiroshima 731-5193, Japan
[5] Faculty of Engineering, Universitas Muhammadiyah Ponorogo, Jl. Budi Utomo No. 10, Ponorogo 63471, Indonesia

E-mail: shimamura@port.kobe-u.ac.jp

Received 3 January 2016, revised 12 February 2016
Accepted for publication 15 February 2016
Published 8 March 2016

Abstract

The atomistic mechanism of dissociative adsorption of ethylene molecules on a Ni cluster is investigated by *ab initio* molecular-dynamics simulations. The activation free energy to dehydrogenate an ethylene molecule on the Ni cluster and the corresponding reaction rate is estimated. A remarkable finding is that the adsorption energy of ethylene molecules on the Ni cluster is considerably larger than the activation free energy, which explains why the actual reaction rate is faster than the value estimated based on only the activation free energy. It is also found from the dynamic simulations that hydrogen molecules and an ethane molecule are formed from the dissociated hydrogen atoms, whereas some exist as single atoms on the surface or in the interior of the Ni cluster. On the other hand, the dissociation of the C-C bonds of ethylene molecules is not observed. On the basis of these simulation results, the nature of the initial stage of carbon nanotube growth is discussed.

Keywords: nickel cluster, ethylene molecule, dissociation, *ab initio* molecular dynamics simulation, activation energy, adsoption energy

(Some figures may appear in colour only in the online journal)

1. Introduction

The growth process of carbon nanotubes (CNTs) [1, 2] has been widely discussed because an understanding of this process is essential for the control of diameter and chirality of CNTs from a point of view of application. In particular, the role of catalytic metal particles and clusters during catalytic chemical vapor deposition (CCVD) [3–5], which is a major technique for CNT synthesis, has been widely discussed [6–9]. The growth of CNTs via CCVD is considered to occur through a series of processes with different spatiotemporal scales. First, carbon precursor molecules, such as ethylene, ethanol, and methane molecules, are dissociated on the surface of catalytic metals and release isolated carbon atoms (or carbon dimers). The isolated carbon atoms form hexagonal networks on the metal surface or within the subsurface of catalytic metals, followed by the formation of a cap structure. The cap structure is gradually lifted up from the catalytic metals, and an elongated tube structure is formed subsequently. Regarding the cap formation process, various atomic simulations, such as classical molecular dynamics (MD) [10–16] and tight-binding based techniques [17–20], have been carried out starting from isolated carbon atoms, and a metal-catalyzed growth model has been proposed [10]. Later, observations by *in-situ* transmission electron microscopy (TEM) [21, 22] have validated this model, and therefore there has been a broad consensus

 © 2016 IOP Publishing Ltd Printed in the UK

up to now that the cap structure is nucleated on the surface of catalytic metal nanoparticles.

With respect to the initial dissociation process, it is well known that the yield and quality of CNT products strongly depend on the choice of carbon precursor molecules and additives. In the CCVD process, carbon monoxide [3, 4], alcohols [5], and hydrocarbons such as methane molecules [23–25] and ethylene molecules [25–27] are mainly employed as carbon precursor molecules. It has been empirically confirmed that the CCVD process using ethanol molecules, called the alcohol CCVD (ACCVD) technique [5], yields a larger amount of single-walled carbon nanotubes (SWNTs) without generation of amorphous carbon compared to the process using the hydrocarbons. Therefore, the presence of a hydroxyl group is considered to enhance the quality of CNTs by eliminating by-products such as amorphous carbon. This idea is backed up by the super growth CVD technique developed by Hata *et al* [28], in which the addition of a small amount of water enhances the activity and lifetime of the catalytic metal drastically and nanotube forests with heights of up to 2.5 mm are repeatedly synthesized.

In order to understand the effect of the carbon precursor molecules and additives described above, it is important to investigate the dissociation process of the carbon precursor molecules on the catalytic metals. Recent *in-situ* mass spectroscopic analysis [29–31] revealed some aspects of the dissociation of carbon precursor molecules during CNT growth by CCVD, in which ethylene molecules and acetylene molecules are key products of the dissociation of ethanol molecules [31]. However, it has not been easy to observe such reaction processes directly during the CCVD process, because it takes place at high temperatures. Therefore, the MD-based simulation is strongly desired for understanding such complicated processes from an atomic point of view. It is, however, also not straightforward to treat the dissociation process by the classical MD simulation because a low-impact force-field, which would describe the dissociation of the carbon precursor molecules on the metal appropriately, has not been established. Therefore, although there have been some attempts to address the dehydrogenation of hydrocarbon molecules using ReaxFF empirical potentials [32, 33] and density-functional tight-binding (DFTB) semi-empirical potentials [34, 35], almost all previous simulations have not taken the initial dissociation process into account but have been limited to the cap formation process starting from isolated carbon atoms [10, 12–17, 19, 20]. That is, the dissociation of the carbon precursor molecules is ignored or assumed to occur immediately on the catalytic metal surface.

Under such circumstances, we have investigated a dissociation process of several carbon precursor molecules on a metal cluster or surface by *ab initio* MD simulations [36–42]. *Ab initio* MD simulation is a very powerful tool because it can treat the dynamics of molecules, including dissociation and charge transfer, consistently without consideration of the reliability of the force-field, although it is computationally more costly than classical MD simulations. However, the recent development of high performance computers has enabled *ab initio* MD simulations of the dissociation of molecules on a metal cluster in a system consisting of several hundred atoms [43–45]. Up to now, we have investigated the dissociation of ethanol molecules on the Ni [36, 37] and Pt [40] clusters to discuss the initial stage of CNT growth by the CCVD technique. It has been revealed that C-C bonds in the CH_xCO fragments ($x = 1$,2, and 3) are preferentially dissociated in the both surface of the Ni and Pt clusters. In addition, the dynamics of the dissociation of methane molecules on Cu(1 1 1) and Ni(1 1 1) surfaces in the initial stage of graphene growth has been studied [38, 39, 41]. The two metal surfaces are typically used for the graphene synthesis. We have demonstrated that there is a great difference in the reactivity of the methane molecules on the two surfaces. Other than the ethanol and methane molecules, ethylene molecule is also commonly used as the carbon precursor molecule. Our previous *ab initio* MD simulations to examine the reaction of the ethylene molecules with the Ni(1 1 1) surface has clarified that the dehydrogenation of the ethylene molecules occur by three different reaction mechanisms [42]. In this study, we investigate the dissociation of ethylene molecules on the Ni cluster, which are one of the typical combinations for the CCVD synthesis of SWNTs. On the basis of the simulation results, the nature of the initial stage of CNT growth in the case of the Ni cluster is discussed.

2. Method of calculation

The electronic states are calculated using the projector-augmented-wave (PAW) method [46, 47] within the framework of density functional theory. The generalized gradient approximation is used for the exchange-correlation energy. We mainly use the PBE functional [48] without spin polarization. The RPBE functional [49] is also used with spin polarization to calculate adsorption energies. Projector functions are generated for the 1*s* state of hydrogen atoms, the 2*s* and 2*p* states of carbon atoms, and the 3*d*, 4*s*, and 4*p* states of nickel atoms. The Γ point is used for Brillouin zone sampling. The plane-wave-cutoff energy of the electronic pseudo-wave functions is 30 Ry and that of the pseudo-charge density is 250 Ry. The DFT-D method is employed for the semi-empirical correction of the van der Waals interaction [50]. The energy functional is minimized iteratively using a preconditioned conjugate-gradient method [51, 52].

We use a system consisting of a Ni_{32} cluster and 37 ethylene molecules (in total 254 atoms) in a cubic supercell of dimensions $15 \times 15 \times 15$ Å^3 under periodic boundary conditions. MD simulations are performed at a temperature of 1500 K in the canonical ensemble using the Nosé-Hoover thermostat technique [53, 54]. The equations of motion are numerically solved via an explicit reversible integrator [55] with a time step of $\Delta t = 0.242$ fs. The total simulation time is 8.13 ps. In the initial configuration, the Ni cluster, which is annealed beforehand at 1500 K, is immersed in liquid ethylene, as shown in figure 1.

A population analysis [56, 57] generalized to the PAW method [58] is used to clarify the change in the bonding properties of atoms associated with the dissociation reaction of ethylene molecules. By expanding the electronic wave

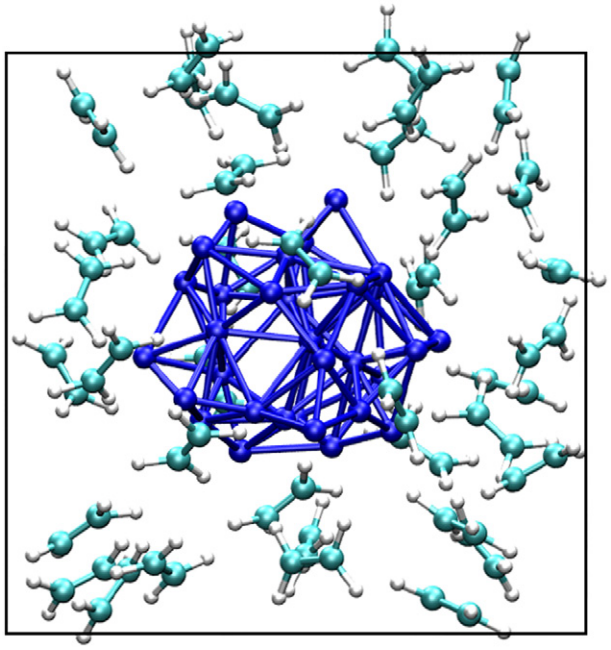

Figure 1. Initial atomic configuration of the system consisting of a Ni_{32} cluster and 37 ethylene molecules.

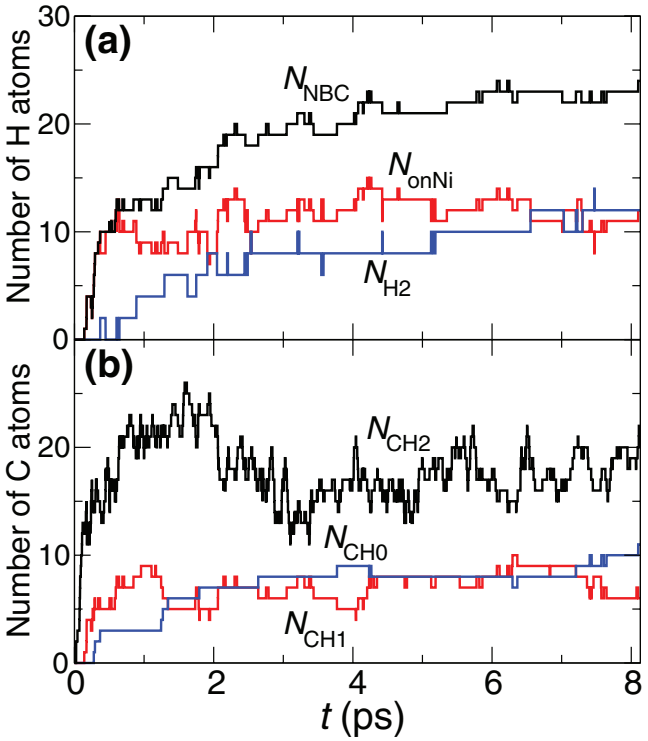

Figure 2. (a) Time evolution of the number of dissociated hydrogen atoms. N_{NBC} represents the number of hydrogen atoms that are not bonded to carbon atoms. N_{H2} represents the number of hydrogen atoms that form hydrogen molecules. N_{onNi} is obtained from $N_{NBC} - N_{H2}$ and corresponds to the number of hydrogen atoms on the Ni cluster. (b) Time evolution of the number of carbon atoms on the Ni cluster. N_{CH2}, N_{CH1} and N_{CH0} represent the number of carbon atoms that are bonded to two, one, and no hydrogen atoms, respectively, as well as to nickel atoms. See text for details of the bond definitions.

functions in an atomic-orbital basis set [59, 60], the bond-overlap populations $O_{ij}(t)$ are obtained for each atomic pair and the gross populations $Z_i(t)$ are obtained for each atom. $O_{ij}(t)$ and $Z_i(t)$ give a semi-quantitative estimate of the covalent-bond strength between atoms and the atomic charge, respectively.

To identify the minimum energy paths and to estimate the activation energies of the chemical reactions found in the MD simulations, the nudged-elastic-band (NEB) method [61, 62] is used. In the NEB method, the reactant configuration $\mathbf{R}_0$ and the product configuration $\mathbf{R}_M$ are connected by a chain consisting of $M-1$ replicas with elastic springs. They are then optimized toward the minimum energy path. In this study, a value of $M = 10$ is used. The initial (reactant) and final (product) configurations are prepared as follows. First, the atomic configurations just before and after the chemical reaction are picked out from the MD simulations. Second, structural optimization of the two systems is performed, and then the systems are used as the initial and final configurations. The intermediate replica configurations are prepared by linear interpolation.

The NEB method explained above gives energy profiles at zero temperature. We also study the effect of finite temperatures on the dehydrogenation and C-C bond dissociation of the ethylene molecule by calculating free energies. We carry out additional *ab initio* MD simulations at temperature $T = 1500$ K by imposing geometrical constraints to obtain the free energy profile [63, 64]. The Lagrange multiplier $\lambda(r)$ is introduced to constrain the distance r between carbon atoms. The relative free energies are obtained by the following integral:

$$\Delta F(r) = \int_{r_0}^{r} \langle \lambda(r') \rangle \mathrm{d}r',$$

where $\langle \lambda(r) \rangle$ is the average of the Lagrange multiplier at r, and r_0 is the equilibrium distance.

The adsorption energy is calculated by subtracting the energy of the Ni_{32} cluster with an adsorbed ethylene molecule from the sum of the energies of an isolated ethylene molecule and an isolated Ni cluster. The potential energies are obtained after their respective structures are optimized. The details of the calculation results are described in section 3.8.

3. Results and discussion

3.1. The number of dissociated hydrogen atoms

The dissociation of ethylene molecules resulting in the release of hydrogen atoms is observed in the simulations. Approximately 20 dehydrogenation reactions occur within 2 ps from the beginning of the simulation, which corresponds to a reaction rate of as much as 10 ps^{-1}. Although some of the dissociated hydrogen atoms are bonded back to carbon atoms, a certain number of them exist without C-H bonding. The time evolution of the number of dissociated hydrogen atoms is shown in figure 2(a), where N_{NBC} represents the number of hydrogen atoms that are not bonded to carbon atoms, N_{H2} represents the number of hydrogen atoms forming hydrogen molecules, and N_{onNi}, which is obtained from $N_{NBC} - N_{H2}$, corresponds to the number of hydrogen atoms on the Ni cluster. Hydrogen and carbon atoms are considered to be

bonded when their distance is less than a cutoff distance R_{CH} during a prescribed bond lifetime τ. Similarly, two hydrogen atoms are considered to be bonded when their distance is less than R_{HH} during τ. Values of $R_{HC} = 1.6$ and $R_{HH} = 1.1$ Å are determined from the first minima of the partial radial distribution functions for H-C and H-H, respectively, and a bond lifetime of $\tau = 24$ fs is used. It should be noted that N_{onNi} fluctuates near ∼12 after 0.5 ps. This result indicates that the number of hydrogen atoms that can exist around the Ni cluster is limited, certainly owing to the finite volume of the Ni cluster. When the number of the hydrogen atoms exceeds the limitation, the extra hydrogen atoms are removed by producing hydrogen molecules.

3.2. Number of carbon atoms on the Ni cluster

We consider that carbon atoms are adsorbed on the Ni cluster when the distance from any of the nickel atoms is less than a cutoff distance R_{CNi} during the prescribed bond lifetime τ. A value of $R_{CNi} = 2.6$ Å is determined from the first minimum position of the partial radial distribution function for C and Ni atoms. The number of carbon atoms on the Ni cluster is classified into three groups according to the number of bonded hydrogen atoms: N_{CH2}, the number of carbon atoms bonded to two hydrogen atoms on the Ni cluster (hereafter, referred as 'C_{H2}'); N_{CH1}, the number of carbon atoms bonded to one hydrogen atom on the Ni cluster ('C_{H1}'); and N_{CH0}, the number of carbon atoms bonded to no hydrogen atom ('C_{H0}'). The time evolution of them is shown in figure 2(b). Since the C-C covalent bonds in the ethylene molecules are not broken even once in the simulations, each carbon atom is bonded to at least one other carbon atom. In addition to this C-C bond, some covalent interaction exists between the carbon and nickel atoms on the cluster. As shown in figure 2(b), N_{CH2} increases rapidly up to 2 ps at which 17 ethylene molecules are adsorbed on the Ni cluster, and the surface of the Ni cluster is saturated. Following this increase in N_{CH2}, C_{H1} and C_{H0} are produced gradually by removing hydrogen atoms from the adsorbed ethylene molecules during this period. From 2 to 3 ps, N_{CH2} decreases, because some of the ethylene molecules are released from the Ni cluster, and some of C_{H2} are converted to C_{H1} and C_{H0}. After 3 ps, several ethylene molecules are newly adsorbed on the Ni cluster. Hence, N_{CH2} gradually rises again. N_{CH1} fluctuates around ∼6 after 0.5 ps. In contrast, N_{CH0} increases monotonically, which indicates that it is difficult to form bonds with hydrogen atoms once a carbon atom becomes C_{H0}. In fact, C_{H0} sinks to the Ni cluster and forms bonds with more nickel atoms, as will be shown later.

3.3. Dehydrogenation process of an ethylene molecule

Figure 3 shows the dehydrogenation of an ethylene molecule on the Ni cluster observed in the simulations. The time evolution of the atomic configuration is shown in figure 3(a), where the breaking of the C1-H1 bond and the formation of C1-nickel bonds are demonstrated. Figure 3(b) shows the time evolution of the bond-overlap populations $O_{ij}(t)$ and the gross populations $Z_i(t)$ for specified atoms. The snapshot at 50 fs

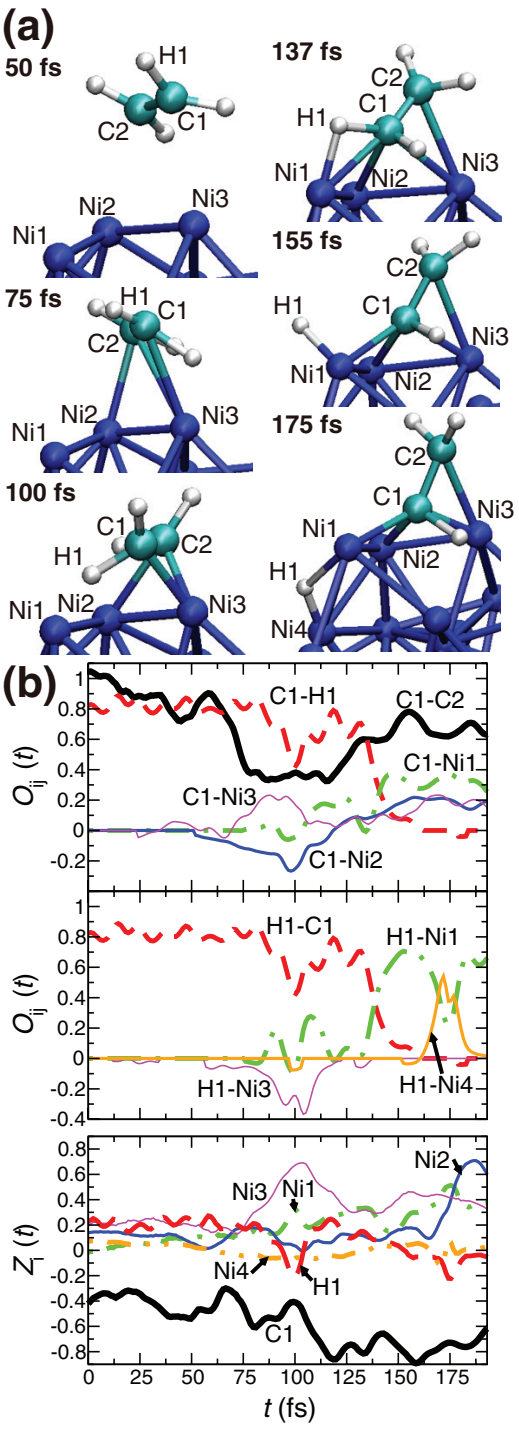

Figure 3. (a) Atomic configurations at 50, 75, 100, 137, 155, and 175 fs during the dehydrogenation of an ethylene molecule on the Ni cluster. (b) Time evolution of the bond-overlap populations $O_{ij}(t)$ and the gross populations $Z_i(t)$ associated with the atoms labeled in (a). Note that $O_{C1-H1}(t)$ and $O_{H1-C1}(t)$ are the same.

represents the atomic configuration before the ethylene molecule is adsorbed on the Ni cluster. It is seen that the C1-C2 pair has a double bond before 70 fs, as $O_{C1-C2}(t)$ has a large value of ∼0.9. However, $O_{C1-C2}(t)$ decreases rapidly to about half its value around 75 fs. This decrease indicates that the bond becomes a single bond, because the C1 atom has some covalent interaction with nickel atoms ($O_{C1-Ni3}(t)$ has finite

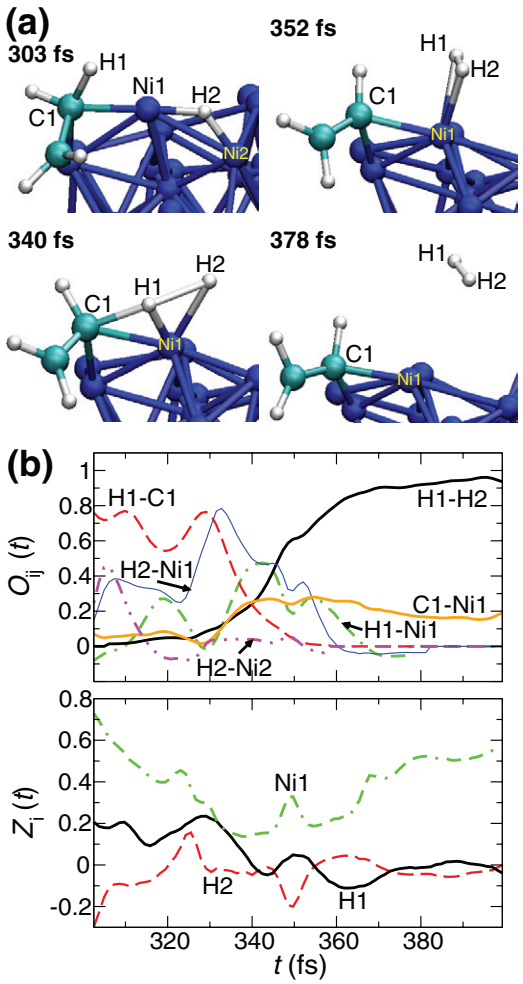

Figure 4. (a) Atomic configurations at 303, 340, 352, and 378 fs during the production of a hydrogen molecule. (b) Time evolution of the bond-overlap populations $O_{ij}(t)$ and the gross populations $Z_i(t)$ associated with the atoms labeled in (a).

values) after 70 fs. When $O_{C1-H1}(t)$ decreases temporarily at about 100 fs, $O_{C1-Ni1}(t)$ and $O_{H1-Ni1}(t)$ begin to increase gradually with some fluctuations. Note that $O_{C1-Ni2}(t)$ and $O_{H1-Ni3}(t)$ have negative values between 50 and 120 fs. At about 130 fs, $O_{C1-H1}(t)$ begins to decrease, and simultaneously $O_{C1-Ni1}(t)$ and $O_{H1-Ni1}(t)$ increase rapidly, which indicates that a bonding state over three atoms (Ni1, H1 and C1) exist. Subsequently, $O_{C1-H1}(t)$ decreases to zero at about 155 fs, i.e. the H1 atom is removed from the molecule, as shown in the snapshot at 155 fs. On the other hand, the strength of the C1-C2 bond is slightly enhanced during this reaction. Near 175 fs, the chemical bond for H1-Ni1 weakens for a short time, and instead, the H1 atom strengthens its bond with the Ni4 atom. In this way, dissociated hydrogen atoms including H1, the number of which corresponds to N_{onNi} in figure 2(a), move around the Ni cluster by exchanging covalent bonds with the nickel atoms.

In terms of the gross population, $Z_{H1}(t)$ is positive before the dehydrogenation reaction ($t < 70$ fs), and then decreases to neutral or a slightly negative value after the reaction ($t > 150$ fs). After the formation of the C-Ni bond, $Z_{C1}(t)$ becomes more negative while $Z_{Ni1}(t)$, $Z_{Ni2}(t)$, and $Z_{Ni3}(t)$ become more positive, indicating that the electrons are transferred from nickel to carbon atoms.

3.4. Production process of hydrogen molecules

As mentioned in section 3.1, hydrogen molecules are produced from the dissociated hydrogen atoms. Two types of mechanisms are involved in the production process depending on the atoms that are bonded to the two hydrogen atoms before the generation of H_2. One type is shown in figure 4. As can be seen in figure 4(a), at 303 fs, one hydrogen atom (H1) is bonded to a carbon atom (C1), and the other hydrogen atom (H2) is bonded to nickel atoms (Ni1 and Ni2) before the production of H_2. These are confirmed by the fact that $O_{H1-C1}(t)$, $O_{H2-Ni1}(t)$, and $O_{H2-Ni2}(t)$ have finite values at $t < 310$ fs (figure 4(b)). The atom H1 forms a bond with Ni1 ($O_{H1-Ni1}(t)$ increases) beginning at 310 fs, and this bond formation leads to the weakening of its bond with C1 ($O_{H1-C1}(t)$ decreases). Moreover, H1 begins to interact with H2 ($O_{H1-H2}(t)$ increases) gradually at about 320 fs, at which H2 is bonded only to Ni1. At about 325 fs, $O_{H2-Ni1}(t)$ and $O_{H1-Ni1}(t)$ begin to increase and decrease, respectively. After they have reached maximum and minimum values, respectively, around 330 fs, $O_{H1-C1}(t)$ as well as $O_{H2-Ni1}(t)$ decrease, while $O_{C1-Ni1}(t)$ as well as $O_{H1-Ni1}(t)$ increase. Until $O_{H1-C1}(t)$ disappears at about 350 fs, a bonding state over four atoms (H1, H2, Ni1, and C1) exists, as shown in the snapshot at 340 fs. After the breaking of the H1-C1 bond, the H1-Ni1 and H2-Ni1 bonds are maintained for a while, as can be seen in the snapshot at 352 fs. Accompanying the decrease in the influence of Ni1 ($O_{H2-Ni1}(t)$ and $O_{H1-Ni1}(t)$ disappear at about 360 fs and 370 fs, respectively), the cohesion of H1-H2 is rapidly enhanced. Finally, after 370 fs, $O_{H1-H2}(t)$ maintains a high value of approximately 0.9, and the sum of $Z_{H1}(t)$ and $Z_{H2}(t)$ becomes nearly zero, which indicates that a hydrogen molecule is formed, as shown in the snapshots at 378 fs.

The other mechanism of hydrogen molecule formation is shown in figure 5. In this case, a hydrogen molecule is generated from two dissociated hydrogen atoms instead of from one that is bonded to a carbon atom, as in the former case. In the snapshot at 2.439 ps, one hydrogen atom (H3) bonds to two nickel atoms (Ni3 and Ni4), and the other hydrogen atom (H4) bonds to two nickel atoms (Ni3 and Ni5), as can be seen in figure 5(a). Since both H3 and H4 approach Ni3, $O_{H3-Ni3}(t)$ and $O_{H4-Ni3}(t)$ increase while $O_{H3-Ni4}(t)$ and $O_{H4-Ni5}(t)$ decrease as shown in figure 5(b). When $O_{C2-Ni3}(t)$ begins to increase gradually at about 2.45 ps, $O_{H3-Ni3}(t)$ and $O_{H4-Ni3}(t)$ begin to decrease, while $O_{H3-H4}(t)$ increases rapidly. Around 2.480 ps, $O_{H3-Ni3}(t)$, $O_{H4-Ni3}(t)$, and $O_{H3-Ni4}(t)$ decrease to zero, and $O_{H3-H4}(t)$ maintains a high value of ~0.9. In this way, a hydrogen molecule is formed as shown in the snapshots at 2.480 and 2.490 ps.

In both these mechanisms of the production of hydrogen molecules, a carbon atom is bonded to a nickel atom and plays a role as a catalyst (C1 in figure 4 and C2 in figure 5). Since the carbon atom attracts the nickel atoms' electrons which form the Ni-H bond, the interaction between a hydrogen molecule and the Ni cluster becomes weak. Whenever the

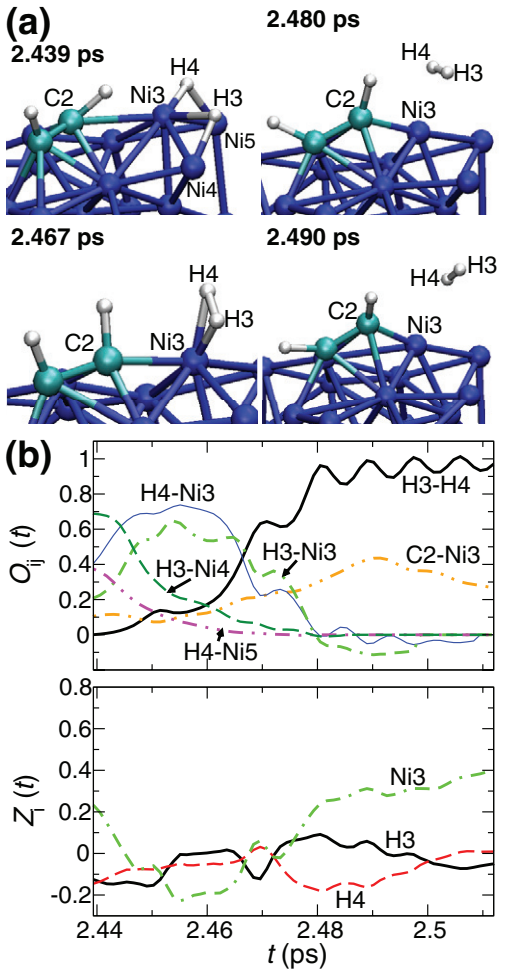

Figure 5. (a) Atomic configurations at 2.439, 2.467, 2.480, and 2.490 ps during the production of a hydrogen molecule. (b) Time evolution of the bond-overlap populations $O_{ij}(t)$ and the gross populations $Z_i(t)$ associated with the atoms labeled in (a).

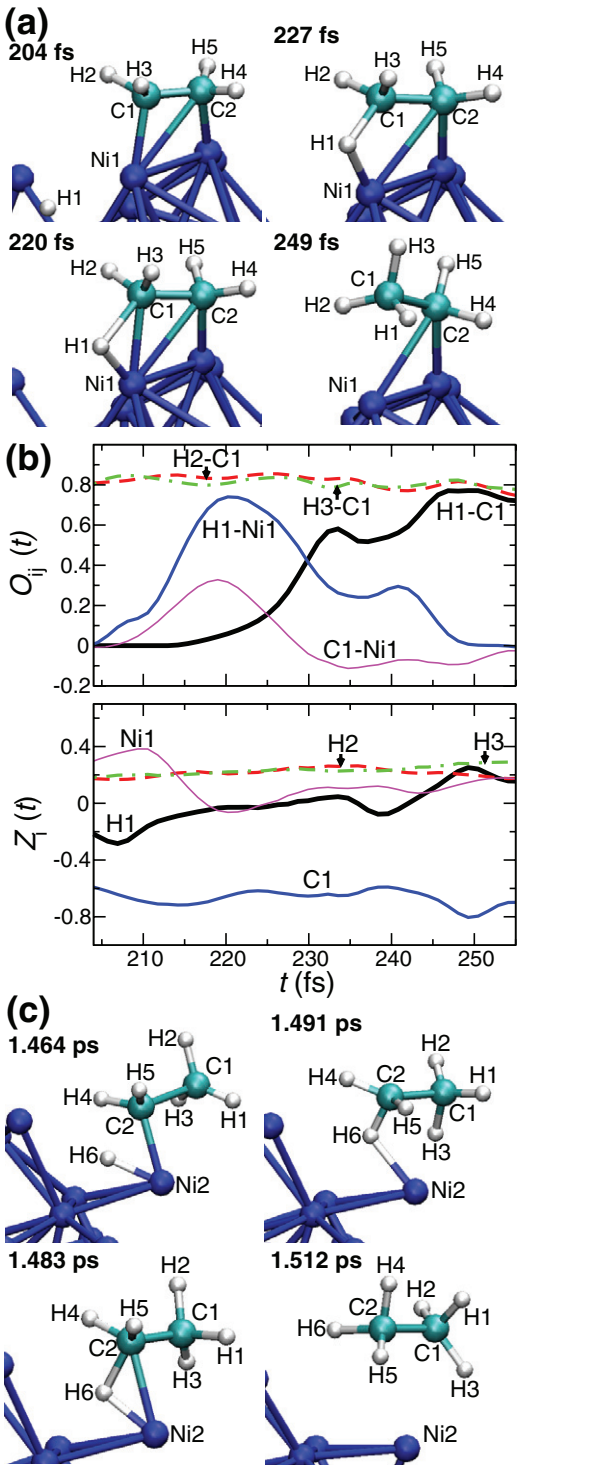

Figure 6. (a) Atomic configurations at 204, 220, 227, and 249 fs during the generation of a CH_3 group (methyl group). (b) Time evolution of the bond-overlap populations $O_{ij}(t)$ and the gross populations $Z_i(t)$ associated with the atoms labeled in (a). (c) Atomic configurations at 1.464, 1.483, 1.491, and 1.512 ps during the generation of an ethane molecule.

bond between the carbon and nickel atoms strengthens, the bond between the hydrogen atoms also strengthens. Therefore, the existence of carbon atoms is essential for the generation of hydrogen molecules.

3.5. Production process of an ethane molecule

The production of C_2H_5 fragments is also observed in the simulations as is demonstrated in figures 6(a) and (b). In the configuration at 204 fs, both H1 and C1 are approaching Ni1 to form a covalent bond ($O_{C1-Ni1}(t)$ and $O_{H1-Ni1}(t)$ begins to increase). At about 220 fs, the chemical bonds of H1-Ni1 and C1-Ni1 begin to weaken, and instead $O_{H1-C1}(t)$ begins to increase. C1 has a fivefold coordination temporarily after 220 fs (see the snapshot at 220 fs), and at about 230 fs, fourfold coordination is recovered by breaking the bond with Ni1 (see the snapshot at 227 fs). Since H1 breaks the bond with Ni1 and $Z_{H1}(t)$ reaches a value similar to that of $Z_{H2}(t)$ and $Z_{H3}(t)$, a C_2H_5 fragment consisting of H1, H2, H3, H4, H5, C1, and C2 is formed, as shown in the snapshot at 249 fs.

In addition, an ethane molecule is generated from the C_2H_5 fragment and a hydrogen atom. The time evolution of the atomic configuration during the formation of an ethane molecule is shown in figure 6(c). In this way, the dissociated hydrogen atoms are also removed from the Ni cluster through the formation of ethane molecules. Although ethane molecules can be carbon precursor molecules, the probability of transforming to

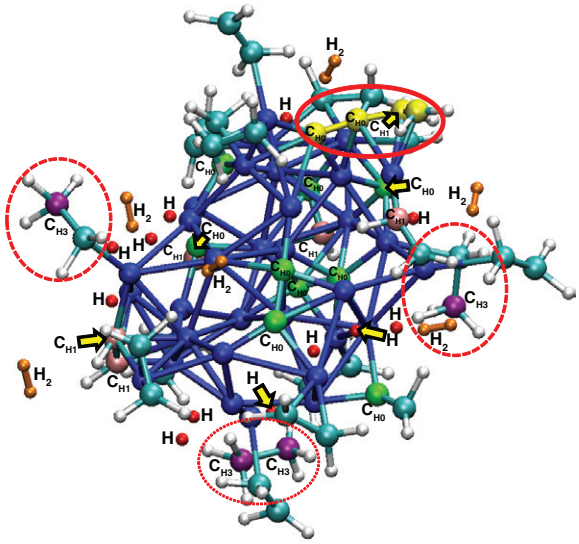

Figure 7. Atomic configuration at 8.13 ps. Spheres labeled 'C_{H3}', 'C_{H1}', and 'C_{H0}' are carbon atoms that are bonded to three, one, and no hydrogen atoms, respectively. Spheres labeled 'H' are dissociated hydrogen atoms. Pairs of spheres labeled 'H_2' are hydrogen molecules. The number of C_{H3}, C_{H1}, C_{H0}, H, and H_2 is 4, 6, 11, 12, and 6, respectively. The open, dashed, and dotted circles indicate a carbon chain with four carbon atoms, two C_2H_5 fragments and an ethane molecule, respectively.

CNT may be small under the situation where there exist many ethylene molecules around because ethane molecules are more stable than ethylene molecules. In fact, the ethane molecule has been present until the end of the simulation.

In total, eight C_2H_5 fragments are formed in the simulations, five of which return to ethylene molecules through removal of one of the bonded hydrogen atoms.

3.6. Atomic configuration

Figure 7 shows a snapshot of the Ni cluster and its surroundings at 8.13 ps, where the ethylene molecules not bonded to the Ni cluster are eliminated. In total, 24 ethylene molecules are adsorbed on the Ni cluster, some of which are dehydrogenated. On the other hand, the breakage of the C-C bonds does not occur even once during the simulations, whereas C-C bonds of ethanol molecules are broken via CH_xCO fragments ($x = 1$, 2, and 3) in our previous siulations [36, 37]. This fact suggests that pairs of carbon atoms are the fundamental elements for the synthesis of CNTs when ethylene molecules are used as the carbon precursor molecules. In fact, a carbon chain consisting of two pairs of carbon atoms is observed, as shown within the open circle in figure 7. It is considered that the formation of the CNT framework can be seen if the additional long-term simulation is carried out. The previous studies regarding the CNT synthesis by the Diels–Alder cycloaddition reaction have also suggested that the pairs of carbon atoms become the direct components [65–67]. In table 1, the numbers of carbon atoms bonded by three, one, and no hydrogen atoms (spheres labeled 'C_{H3}', 'C_{H1}', and 'C_{H0}', respectively in figure 7) as well as the number of carbon atoms that bond to two hydrogen atoms.

Table 1. The numbers n of carbon atoms, C_2H_x fragments or molecules, hydrogen atoms, and hydrogen molecules shown in figure 7.

Carbon atom	n	Fragment or molecule	n	Atom or molecule	n
C_{H3}	4	C_2H_0	3	H	12
C_{H2}	27	C_2H_1	2	H_2	6
C_{H1}	6	C_2H_2	4		
C_{H0}	11	C_2H_3	2		
		C_2H_4	10		
		C_2H_5	2		
		C_2H_6	1		

Note: $C_{H}x$ indicates the carbon atom bonding to x hydrogen atoms.

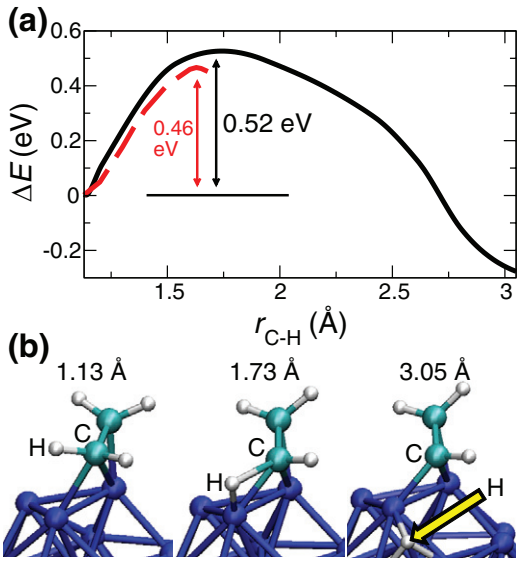

Figure 8. (a) Energy profile along the reaction path of the dehydrogenation reaction of an ethylene molecule on the Ni cluster as a function of the distance r_{C-H} between the carbon and hydrogen atoms whose bond is broken, obtained by NEB calculation. The dashed curve is the free-energy profile at 1500 K. (b) Atomic configurations at $r_{C-H} = 1.13$ Å (initial), 1.73 Å (barrier), and 3.05 Å (final).

Furthermore, the dissociated hydrogen atoms exist on the surface or in the interior of the Ni cluster (spheres labeled 'H'), or form hydrogen molecules (spheres labeled 'H_2'), C_2H_5 fragments (shown in the dashed circles) and an ethane molecule (shown in the dotted circle) as described in the previous sections 3.1 and 3.5. The numbers of C_2H_x fragments, hydrogen atoms, and hydrogen molecules are also listed in table 1.

3.7. Activation energy of dehydrogenation of an ethylene molecule

The activation energies of the chemical reactions observed in the MD simulations are estimated by the NEB method. The calculation method is introduced in section 2. The activation energy for removal of a hydrogen atom from an ethylene molecule on the Ni cluster, which was described in section 3.3, is calculated first as shown in figure 8. Figure 8(a) shows the energy profile, and the initial, barrier, and final configurations

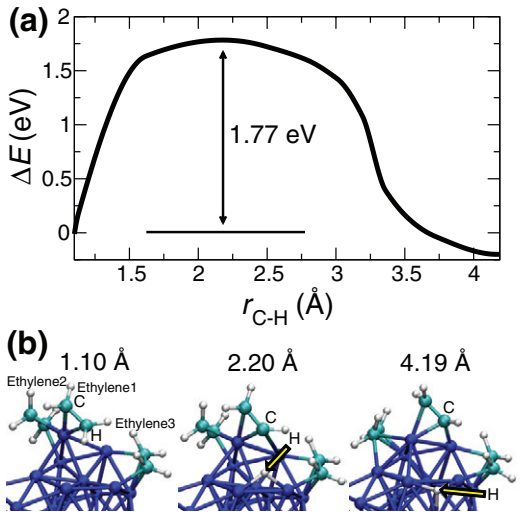

Figure 9. (a) Energy profile along the reaction path of the dehydrogenation reaction involving three ethylene molecules on the Ni cluster as a function of the distance r_{C-H} between the carbon and hydrogen atoms whose bond is broken, obtained by NEB calculation. (b) Atomic configurations at $r_{C-H} = 1.10$ Å (initial), 2.20 Å (barrier), and 4.19 Å (final).

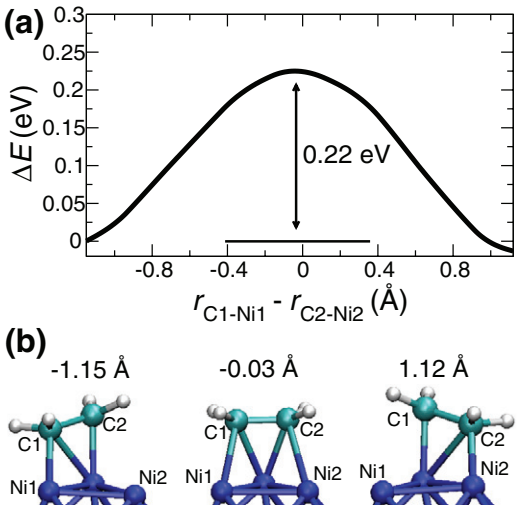

Figure 10. (a) Energy profile along the migration path of an ethylene molecule on the Ni cluster as a function of the difference $r_{C1-Ni1} - r_{C2-Ni2}$ between two C-Ni distances, obtained by NEB calculation. (b) Atomic configurations at $r_{C1-Ni1} - r_{C2-Ni2} = -1.15$ Å (initial), −0.03 Å (barrier), and 1.12 Å (final).

are shown in the left, middle, and right panels of figure 8(b), respectively. The activation energy for the reaction is estimated to be 0.52 eV. The minimum energy paths for several processes are identified, and it is found that most of the dehydrogenation reactions essentially involve only one ethylene molecule and the Ni cluster, as shown in figure 8. However, very rarely, the dehydrogenation reactions involving more than one ethylene molecule occur. Figure 9 shows a reaction involving three ethylene molecules on the Ni cluster. Figure 9(a) shows the energy profile, and the initial, barrier, and final configurations are shown in the left, middle, and right panels of figure 9(b), respectively. As can be seen in figure 9(b), the hydrogen atom labeled 'H' of 'ethylene1' is removed. 'ethylene2' is responsible for tilting ethylene1 toward the front side of the paper. When the structural optimization is performed without ethylene2, both carbon atoms of ethylene1 are placed on one nickel atom as will be shown in figure 12(a), which does not represent the actual atomic configuration of the dehydrogenation process. In addition, the shape of the Ni cluster is largely deformed without ethylene3. It is not until the two ethylene molecules (ethylene2 and ethylene3), which are not dehydrogenated, are considered that the actual dehydrogenation reaction identified in the MD simulations could be followed by the NEB. The activation energy amounts to 1.77 eV. This value is much higher than that for the reaction involving only one ethylene molecule, because the hydrogen atom that is removed moves toward Ni atoms that are not bonded to the carbon atoms.

It is also observed in the MD simulations that some ethylene molecules on the Ni cluster change their positions without dehydrogenation. Figure 10 shows the energy profile when an ethylene molecule moves between two stable sites on the Ni cluster. Figure 10(a) shows the energy profile, and the initial, barrier, and final configurations are shown in the left, middle, and right panels of figure 10(b), respectively.

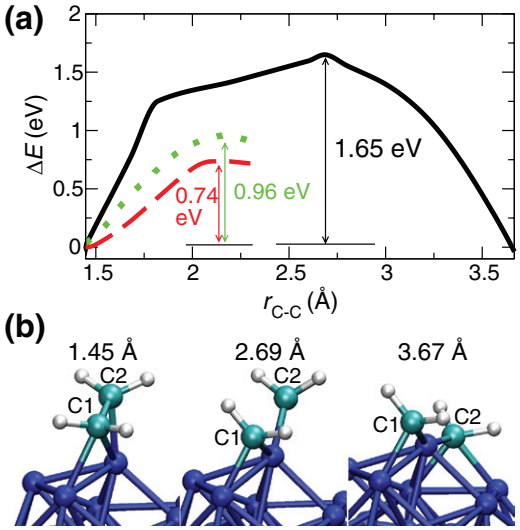

Figure 11. (a) Energy profile (solid curve) along the reaction path of the dissociation reaction of a C-C bond of an ethylene molecule on the Ni cluster as a function of the distance r_{C-C} between the two carbon atoms whose bond is broken, obtained by NEB calculation. The dashed curve is the free-energy profile at 1500 K. The dotted curve is the free-energy profile at 1500 K for the C-C dissociation of a CH_2-CH fragment on the Ni cluster. (b) Atomic configurations at $r_{C-C} = 1.45$ Å (initial), 2.64 Å (barrier), and 3.67 Å (final).

The activation energy for this movement is estimated to be 0.22 eV.

To investigate the stability of the covalent bond between carbon atoms, we calculate the activation energy for the dissociation of a C-C bond of an ethylene molecule on the Ni cluster. Figure 11 shows the energy profile of the dissociation reaction of the C-C bond. Figure 11(a) shows the energy profile, and the initial, barrier, and final configurations are shown in the left, middle, and right panels of figure 11(b), respectively. We have obtained the activation energy of 1.68 eV. The corresponding reaction rate is estimated as

$k = (k_B T/h)\exp(-\Delta E/k_B T) = 7.10 \times 10^{-5}$ ps^{-1}at 1500 K according to transition state theory [68], where k_B is the Boltzmann constant, h is the Planck constant, and ΔE is the activation energy. On the other hand, the activation energy of 0.52 eV for the dehydrogenation reaction shown in figure 8 corresponds to the reaction rate of 0.56 ps^{-1} at 1500 K. Thus, the activation energy of the C-C dissociation is more than three times lager, and the corresponding reaction rate is five order of magnitude smaller than the C-H dissociation. The C-C bonds are much more stable than the C-H bonds. Furthermore, we estimate the finite-temperature effects on the dehydrogenation and dissociation of the C-C bond using the calculation method introduced in section 2. The activation free energies are 0.46 and 0.74 eV as shown by the dashed lines in figures 8(a) and 11(a), the corresponding reaction rates of which are 0.89 and 0.10 ps^{-1}, respectively. Although the energy barrier for the C-C dissociation becomes less than half by the finite temperature effect, the value is still much larger than the activation free energy of the dehydrogenation reaction, and the corresponding reaction rate is very small. Moreover, we have observed that the strength of the C-C bond becomes larger after the dehydrogenation occurs as shown in figure 3. To confirm this from the point of view of finite-temperature effect, the activation free energy is calculated using the system consisting of a dehydrogenated ethylene molecule, i.e. a CH_2-CH fragment, and the Ni cluster. The energy is 0.96 eV as shown by the dotted line in figure 11(a) and the corresponding reaction rate is 0.02 ps^{-1}. Since the reaction rate becomes much smaller than the rate of the C-C dissociation of the ethylene molecule, it is concluded that the probability of the dissociation of the C-C bond is very small.

3.8. Adsorption energy of an ethylene molecule on the Nicluster

In section 3.7, it was shown that the activation free energy for the dehydrogenation reaction involving one ethylene molecule is of the order of 0.46 eV, and the corresponding reaction is extimated as 0.89 ps^{-1} at 1500 K. However, dehydrogenation reactions have been observed to proceed at a faster rate of about 10 ps^{-1} as mentioned in section 3.1, which indicates that a larger energy is supplied to the ethylene molecules so that they can readily overcome the energy barrier of 0.46 eV. We expect that the adsorption energy of the ethylene molecules on the Ni cluster is the source of the energy. The method of the calculation of the adsorption energy is introduced in section 2. Figures 12(a)–(d) show selected adsorption sites on the Ni cluster that have adsorption energies in the range of approximately 1.5–1.7 eV. These results indicate that an amount of energy considerably larger than the activation free energy of 0.46 eV is supplied to the ethylene molecules when they are adsorbed on the Ni cluster. Thus, it is concluded that the dehydrogenation rate is enhanced by the adsorption energy. In addition, the adsorption site in figure 12(c) is the most often observed in our MD simulation. The site may be preferred under the circumstance that there are several ethylene molecules.

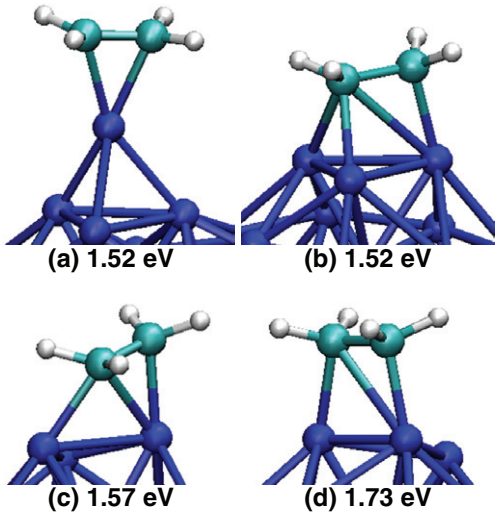

Figure 12. Atomic configurations for four different adsorption sites of ethylene molecules on the Ni cluster. The values of their respective adsorption energies are also shown.

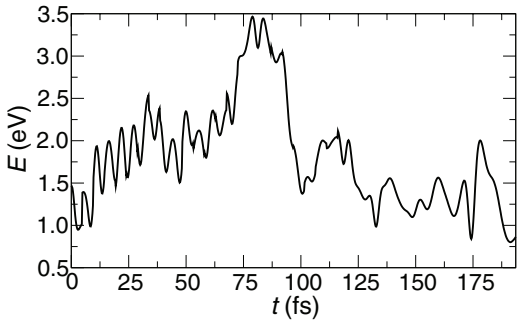

Figure 13. Time evolution of the kinetic energy of the ethylene molecule for which we have discussed its dehydrogenation reaction in section 3.3.

To estimate the adsorption energy at the finite temperature, we calculate the kinetic energies of the ethylene molecule for which we have discussed its dehydrogenation reaction in section 3.3 (see figure 3), as shown in figure 13. The initial kinetic energy is about 1.2 eV, which corresponds to 1500 K, i.e. 1.2 (eV) $\sim 1.5 \times k_B \times 1500$ (K) $\times$ 6 (atoms/molecule). When the ethylene molecule approaches the cluster, the kinetic energy rapidly increases, and then shows a peak energy in the range of 2.9–3.4 eV around 80 fs. The energy difference of 1.7–2.2 eV corresponds to the adsorption energy at 1500 K, which is the similar value to the adsorption energies of 1.5–1.7 eV at 0 K, and is much greater than the activation free energy for the dehydrogenation reaction of 0.46 eV.

It should be noted that our previous study [42] has shown the adsorption energy of an ethylene molecule on the Ni(1 1 1) surface is calculated as 0.76 eV, which is only about half of the energy obtained in this study. This means that the reactivity of the Ni cluster is much higher than that of the Ni(1 1 1) surface. The high reactivity leads to many differences in the chemical reactions, such as hydrogen- and ethane-production reactions as well as dehydrogenation reactions. Whereas, in total, about 10 hydrogen atoms are dissociated on the Ni(1 1 1) surface, about 20 atoms are dissociated on the Ni cluster

(see N_{NBC} in figure 2(a)). The number of nickel atoms on the cluster surface is 29, while that on the (1 1 1) surface is 30 [42]. The number of the dissociated hydrogen atoms per 10 surface-nickel atoms is 7 on the cluster, which is about two times larger than that on the (1 1 1) surface. Furthermore, the production of the hydrogen and ethane molecules has never seen on the Ni(1 1 1) surface.

It has been known that the RPBE functional gives more correct results for the adsorption energy than other exchange-correlation functionals [69]. Vang *et al* have calculated the adsorption energy of an ethylene molecule on the Ni surface using the RPBE functional [49] with spin polarization. The adsorption energies obtained for the Ni(1 1 1) and Ni(2 1 1) surfaces are 0.16 and 0.76 eV, respectively [70, 71]. Note that there are steps in the case of the Ni(2 1 1) surface. Since the reactivity of such step sites is higher than the flat Ni(1 1 1) surface, the adsorption energy for the Ni(2 1 1) surface is larger than that for the Ni(1 1 1) surface by 0.6 eV. We also calculate the adsoption energy of an ethylene molecule on the Ni cluster using the RPBE functional with spin polarization. The adsorption energy for the site shown in figure 12(c), which appears most frequently in the MD simulation, is 1.21 eV. Our result shows that the Ni cluster is more reactive than the Ni surfaces, because the adsorption energy is larger than those for the surfaces. Although the value is smaller than that calculated by the PBE functional, it is still considerably larger than the activation energy for the dehydrogenation reaction. Therefore, our conclusion for the enhancement of the dehydrogenation rate due to the adsorption energy is not changed.

4. Conclusions

We have examined the microscopic mechanism of the dissociation reaction of ethylene molecules on a Ni cluster by means of *ab initio* MD simulations. The dissociated hydrogen atoms are present around the Ni cluster as single hydrogen atoms. When the number of hydrogen atoms exceeds the limit imposed by the finite volume of the Ni cluster, hydrogen molecules are generated. In addition, some of the dissociated hydrogen atoms form C_2H_5 fragments; furthermore, an ethane molecule is formed. It was therefore concluded that the dissociated hydrogen atoms are removed from the circumference of the Ni cluster through the formation of ethane molecules as well as hydrogen molecules. The activation free energy for the representative dehydrogenation reaction of an ethylene molecule was estimated to be 0.46 eV, which corresponds to a reaction rate of 0.89 ps^{-1}. However, it was found that the adsorption energy of the ethylene molecules on the Ni cluster is approximately three times larger than the activation energy, which explains why the actual reaction rate is faster than the value estimated based on only the activation energy. On the other hand, no C-C bonds of the ethylene molecules are dissociated during the simulation. Moreover, the formation of a carbon chain via the connection of two pairs of carbon atoms was observed. These facts suggest that the fundamental elements for the synthesis of CNTs are pairs of carbon atoms when the ethylene molecules are used as the carbon precursor molecules.

Acknowledgment

The financial support of KAKENHI (23340106 and 24686026) is gratefully acknowledged. In addition, this work was also partly supported by grant-in-aid for JSPS research fellows 15J01350. The computational support for this work was provided by the Research Institute for Information Technology, Kyushu University. The authors also kindly acknowledge the Supercomputer Center, Institute for Solid State Physics, The University of Tokyo, for the use of its facilities.

References

[1] Iijima S 1991 *Nature* **354** 56
[2] Iijima S and Ichihashi T 1993 *Nature* **363** 603
[3] Dai H, Rinzler A G, Nikolaev P, Thess A, Colbert D T and Smalley R E 1996 *Chem. Phys. Lett.* **260** 471
[4] Nikolaev P, Bronikowski M J, Bradley R K, Rohmund F, Colbert D T, Smith K A and Smalley R E 1999 *Chem. Phys. Lett.* **313** 91
[5] Maruyama S, Kojima R, Miyauchi Y, Chiashi S and Kohno M 2002 *Chem. Phys. Lett.* **360** 229
[6] Banhart F 2009 *Nanoscale* **1** 201
[7] Shibuta Y 2011 *Diamond Relat. Mater.* **20** 334
[8] Journet C, Picher M and Jourdain V 2012 *Nanotechnology* **23** 142001
[9] Neyts E C 2012 *J. Vac. Sci. Technol.* **30** 030803
[10] Shibuta Y and Maruyama S 2003 *Chem. Phys. Lett.* **382** 381
[11] Shibuta Y and Elliott J A 2006 *Chem. Phys. Lett.* **427** 365
[12] Shibuta Y and Maruyama S 2007 *Chem. Phys. Lett.* **437** 218
[13] Shibuta Y and Maruyama S 2007 *Comput. Mater. Sci.* **39** 842
[14] Ding F, Rosén A and Bolton K 2004 *J. Chem. Phys.* **121** 2775
[15] Zhao J, Martinez-Limia A and Balbuena P B 2005 *Nanotechnology* **16** S575
[16] Neyts E C, Shibuta Y, Van Duin A C T and Bogaerts A 2010 *ACS Nano* **4** 6665
[17] Amara H, Bichara C and Ducastelle F 2008 *Phys. Rev. Lett.* **100** 056105
[18] Diarra M, Amara H, Ducastelle F and Bichara C 2012 *Phys. Status Solidi* B **249** 2629
[19] Ohta Y, Okamoto Y, Irle S and Morokuma K 2008 *ACS Nano* **2** 1437
[20] Page A J, Irle S and Morokuma K 2010 *J. Phys. Chem.* C **114** 8206
[21] Hofmann S *et al* 2007 *Nano Lett.* **7** 602
[22] Yoshida H, Takeda S, Uchiyama T, Kohno H and Homma Y 2008 *Nano Lett.* **8** 2082
[23] Cassell A M, Raymakers J A, Kong J and Dai H 1999 *J. Phys. Chem.* B **103** 6484
[24] Colomer J F, Stephan C, Lefrant S, Van Tendeloo G, Willems I, Kónya Z, Fonseca A, Laurent C and Nagy J B 2000 *Chem. Phys. Lett.* **317** 83
[25] Cheung C L, Kurtz A, Park H and Lieber C M 2002 *J. Phys. Chem.* B **106** 2429
[26] Hafner J H, Bronikowski M J, Azamian B R, Nikolaev P, Rinzler A G, Colbert D T, Smith K A and Smalley R E 1998 *Chem. Phys. Lett.* **296** 195
[27] Che G, Lakshmi B B, Martin C R, Fisher E R and Ruoff R S 1998 *Chem. Mater.* **10** 260
[28] Hata K, Futaba D N, Mizuno K, Namai T, Yumura M and Iijima S 2004 *Science* **306** 1362
[29] Inoue S and Maruyama S 2008 *Japan. J. Appl. Phys.* **47** 1931
[30] Tomie T, Inoue S and Matsumura Y 2012 *Chem. Phys. Lett.* **533** 56
[31] Tomie T, Inoue S, Iba Y and Matsumura Y 2012 *Chem. Phys. Lett.* **536** 104

[32] Khalilov U, Bogaerts A and Neyts E C 2014 *Nanoscale* **6** 9206
[33] Mueller J, Van Duin A and Goddard W III 2010 *J. Phys. Chem.* C **114** 5675
[34] Wang Y, Gao X, Qian H J, Ohta Y, Wu X, Eres G, Morokuma K and Irle S 2014 *Carbon* **72** 22
[35] Page A J, Ding F, Irle S and Morokuma K 2015 *Rep. Prog. Phys.* **78** 036501
[36] Oguri T, Shimamura K, Shibuta Y, Shimojo F and Yamaguchi S 2014 *Chem. Phys. Lett.* **595–6** 185
[37] Oguri T, Shimamura K, Shibuta Y, Shimojo F and Yamaguchi S 2013 *J. Phys. Chem.* C **117** 9983
[38] Shibuta Y, Arifin R, Shimamura K, Oguri T, Shimojo F and Yamaguchi S 2014 *Chem. Phys. Lett.* **610–1** 33
[39] Shibuta Y, Arifin R, Shimamura K, Oguri T, Shimojo F and Yamaguchi S 2013 *Chem. Phys. Lett.* **565** 92
[40] Shibuta Y, Shimamura K, Arifin R and Shimojo F 2015 *Chem. Phys. Lett.* **636** 110
[41] Arifin R, Shibuta Y, Shimamura K and Shimojo F 2015 *Eur. Phys. J.* B **88** 303
[42] Arifin R, Shibuta Y, Shimamura K, Shimojo F and Yamaguchi S 2015 *J. Phys. Chem.* C **119** 3210
[43] Shimamura K, Shimojo F, Kalia R, Nakano A, Nomura K I and Vashishta P 2014 *Nano Lett.* **14** 4090
[44] Ohmura S, Shimojo F, Kalia R K, Kunaseth M, Nakano A and Vashishta P 2011 *J. Chem. Phys.* **134** 244702
[45] Shimojo F, Ohmura S, Kalia R K, Nakano A and Vashishta P 2010 *Phys. Rev. Lett.* **104** 126102
[46] Blöchl P E 1994 *Phys. Rev.* B **50** 17953
[47] Kresse G and Joubert D 1999 *Phys. Rev.* B **59** 1758
[48] Perdew J P, Burke K and Ernzerhof M 1996 *Phys. Rev. Lett.* **77** 3865
[49] Hammer B, Hansen L and Nørskov J K 1999 *Phys. Rev.* B **59** 7413
[50] Gómez-Gualdrón D A, McKenzie G D, Alvarado J F J and Balbuena P B 2012 *ACS Nano* **6** 720
[51] Kresse G and Hafner J 1994 *Phys. Rev.* B **49** 14251
[52] Shimojo F, Kalia R K, Nakano A and Vashishta P 2001 *Comput. Phys. Commun.* **140** 303
[53] Nosé S 1984 *Mol. Phys.* **52** 255
[54] Hoover W G 1985 *Phys. Rev.* A **31** 1695
[55] Tuckerman M, Berne B J and Martyna G J 1992 *J. Chem. Phys.* **97** 1990
[56] Mulliken R S 1955 *J. Chem. Phys.* **23** 1833
[57] Mulliken R S 1955 *J. Chem. Phys.* **23** 1841
[58] Shimojo F, Nakano A, Kalia R K and Vashishta P 2008 *Phys. Rev.* E **77** 066103
[59] Daniel S P, Emilio A and José M S 1996 *J. Phys.: Condens. Matter* **8** 3859
[60] Segall M D, Shah R, Pickard C J and Payne M C 1996 *Phys. Rev.* B **54** 16317
[61] Jónsson H, Mills G and Jacobsen K W 1998 *Nudged Elastic Band Method for Finding Minimum Energy Paths of Transitions Classical and Quantum Dynamics in Condensed Phase Simulations* (Singapore: World Scientific)
[62] Henkelman G and Jónsson H 2000 *J. Chem. Phys.* **113** 9978
[63] Hass K, Schneider W, Curioni A and Andreoni W 1998 *Science* **282** 265
[64] Curioni A, Sprik M, Andreoni W, Schiffer H, Hutter J and Parrinello M 1997 *J. Am. Chem. Soc.* **119** 7218
[65] Fort E H, Donovan P M and Scott L T 2009 *J. Am. Chem. Soc.* **131** 16006
[66] Mojica M, Méndez F and Alonso J A 2013 *Molecules* **18** 2243
[67] Jasti R and Bertozzi C R 2010 *Chem. Phys. Lett.* **494** 1
[68] Truhlar D G, Garrett B C and Klippenstein S J 1996 *J. Phys. Chem.* **100** 12771
[69] Hammer B and Nørskov J K 2000 *Adv. Catal.* **45** 71
[70] Vang R T, Honkala K, Dahl S, Vestergaard E, Schnadt J, Læ gsgaard E, Clausen B, Nørskov J K and Besenbacher F 2005 *Nat. Mater.* **4** 160
[71] Vang R, Honkala K, Dahl S, Vestergaard E, Schnadt J, Læ gsgaard E, Clausen B, Nørskov J and Besenbacher F 2006 *Surf. Sci.* **600** 66